İSTANBUL UNIVERSITY CERRAHPAŞA

ORIGINAL ARTICLE
Electrica 2025; 25: 1-13

Design and Simulation Analysis of Source-Grid-Load-Storage Integrated Scheduling for Large-Scale Power Systems

Qideng Luo, Yue Wu, Chunli Zhou, Deyan Zhu

Guangxi Power Grid Co., Ltd, Nanning, China

Cite this article as: Q. Luo, Y. Wu, C. Zhou, and D. Zhu, "Design and simulation analysis of source-grid-load-storage integrated scheduling for large-scale power systems," *Electrica*, 25, 0138, 2025. doi: 10.5152/electrica.2025.24138.

WHAT IS ALREADY KNOWN ON THIS TOPIC?

- *Energy hubs are crucial for achieving efficient energy utilization, supply-demand balance, and integrated scheduling.*
- *Random fuzzy theory can be used to deal with the uncertainty and fuzziness of new energy output.*
- *Use different scheduling models to handle the complex scheduling of large-scale power systems.*

WHAT THIS STUDY ADDS ON THIS TOPIC?

- *By using the random fuzzy power flow algorithm, research can more accurately handle the uncertainty and fuzziness of new energy output, thereby improving*

Corresponding Author:
Qideng Luo

E-mail:
19968283524@163.com

Received: October 17, 2024
Revision Requested: January 11, 2025
Last Revision Received: May 13, 2025
Accepted: May 17, 2025
Publication Date: September 16, 2025

DOI: 10.5152/electrica.2025.24138

ABSTRACT

With the rapid development of new power systems and global energy transformation, the comprehensive scheduling difficulty of large-scale power systems continues to increase. The research aims to design a comprehensive scheduling model to optimize the balance between energy supply and demand, efficiently utilizing electricity. This study establishes an energy control hub and performs random fuzzy power flow calculations. The alternating direction multiplier algorithm is used for regional decentralized calculation in three-layer scheduling programming. Then, a source-grid-load-storage integrated scheduling model based on the alternating direction multiplier algorithm is designed. According to the verification results, the designed model had the lowest abandoned wind and solar rates, which were 7.4% and 2.6%, respectively. During peak shaving periods, the frequency remained stable at around 49.72 Hz, and the demand response at the load side helped reduce frequency drops. The overall cost was 11.7% lower than that of the large-scale power system scheduling model based on Benders. The results indicate that the scheduling model designed for large-scale power systems can flexibly and efficiently integrate source-grid-load-storage scheduling, achieving efficient energy utilization and supply-demand balance. The research designs a new solution for the efficient and flexible operation of large-scale power systems.

Index Terms–ADMM, electricity, distributed, power flow, source-grid-load-storage

I. INTRODUCTION

With the widespread access to distributed new energy and the rapid growth of electricity demand, power system scheduling is becoming increasingly difficult in ensuring the efficient and flexible operation of modern power systems [1]. The access to distributed power sources is also affected by issues such as insufficient grid regulation capacity and large voltage fluctuations. The high penetration rate of distributed power sources exacerbates the random fluctuations on the generation side, increases issues such as overvoltage and power reversal in the distribution network, and disrupts the planning and operation mode of traditional power grids. Energy hubs can effectively balance the volatility and uncertainty of distributed power sources. For example, as a part of the energy hub, microgrids can coordinate and control distributed power sources, energy storage devices, and loads. Therefore, the research aims to design an integrated scheduling model that comprehensively considers power generation, transmission, consumption, and energy storage. Through vertical regulation from generation to consumption and horizontal scheduling between regions and equipment, the power system can operate with high quality and stability [2]. The power system scheduling method based on deep learning algorithms can achieve multi-objective economic scheduling and minimize regional economic costs and pollution emissions, but this method does not consider the energy reserve situation in large-scale power generation [3]. The energy sources, power grids, electricity loads, and energy storage systems in the power system are organically integrated to form a comprehensive energy system, optimize the balance between energy supply and demand, and achieve efficient energy utilization.

Fuzzy Theory (FT) can handle the fuzziness of problems, which makes it more effective in dealing with complex systems and uncertainty problems. In addition, it has the advantages of simple

the reliability and accuracy of scheduling decisions.

- *By using alternating direction multiplier–based optimization methods, research can determine the optimal scheduling strategy, significantly reduce system costs, and improve the consumption capacity of new energy.*
- *Through the three-layer scheduling programming method, flexible scheduling of multi-regional power systems has been studied and implemented, optimizing supply and demand balance and improving the overall operational efficiency of the system.*

design and wide applicability [4]. The alternating direction multiplier (ADMM) algorithm is widely used in the field of optimization. The ADMM introduces an augmented Lagrangian function to transform constrained problems into unconstrained problems, simplifying the solution process of constrained optimization problems. It has high computational efficiency and distributed optimization [5]. Many researchers have conducted related research on the source-grid-load-storage integrated scheduling, FT, ADMM, and large-scale power system scheduling.

Gao et al. proposed a hierarchical network control architecture to address the difficult control of distributed new energy grid connections. The control architecture involved three layers, including the energy management layer, bus control layer, and inverter control layer. The results indicated that the control method had flexible control capabilities in the simulation testing of PSCAD/EMTDC [6]. To solve the instability in large-scale power systems caused by the continuous increase of distributed power sources, Wang et al. developed a MMG (Multi-Microgrid) control strategy to avoid passive transition from grid-connected operation to islanded operation. The research method was effective [7]. Echreshavi et al. proposed a fuzzy static output feedback control scheme to address the information packet loss, time delay, and execution failure in the TSFM control model. The proposed control method reduced fault problems by 37.2%. This method solved the information packet loss, time delay, and execution failure in the control process [8]. To address the insufficient landslide data for accurate landslide risk assessment, Shano et al. designed a landslide risk assessment method based on hazardous pixels and fuzzy set theory. The results showed that the method divided the research area into 6.86% of very high-risk areas, 21.15% of high-risk areas, 43.26% of medium-risk areas, 10.97% of low-risk areas, and 17.76% of extremely low-risk areas [9]. Bai et al. designed a distributed control method based on ADMM to address the stable regulation of Wind Turbines (WTs) in wind farms. This method achieved stable power output inside the WT, and the voltage stabilization performance was improved by 12.6% [10]. To enhance the optimization performance of optimization algorithms in deep learning, Na proposed a gradient learning rate adaptive hierarchical algorithm based on ADMM. The results indicated that the research algorithm outperformed other algorithms in image classification tasks on the benchmark dataset [11]. Shi et al. developed a power resource dynamic programming strategy based on FRDDP (Fast Robust Dual Dynamic Programming) to address the economic dispatch difficulties caused by the integration of distributed energy into the grid. The results showed that the research algorithm reduced the operating cost by 8.67% and exhibited good scalability in large-scale power systems [12]. To solve the large-scale power outages caused by substation shutdowns, Jiang et al. developed a three-stage optimization algorithm for load transfer in distribution systems. Case analysis showed that the algorithm ensured the reliability of important loads and safe operation, while also improving the load recovery rate and enhancing

TABLE I. COMPARISON BETWEEN THE LATEST RESEARCH RESULTS AND RESEARCH CONTENT

Research Contents	Reference	Research Method	The Innovation of This Article
Distributed new energy grid connection control	Gao et al [6]	Hierarchical network control architecture	This article combines random fuzzy theory and ADMM to achieve integrated scheduling of multi-regional source-grid-load-storage
Distributed new energy grid connection control	Wang et al [7]	Control method based on MMG	This article proposes a three-layer scheduling model based on ADMM to optimize scheduling efficiency
Fuzzy control method	Echreshavi et al [8]	Fuzzy static output feedback control	This article uses random fuzzy power flow calculation to improve the reliability of scheduling decisions
Landslide risk assessment	Shano et al [9]	Risk assessment based on fuzzy set theory	This article does not cover
Wind turbine control	Bai et al [10]	Distributed control based on ADMM	This article applies ADMM to the integrated scheduling of source-grid-load-storage in large-scale power systems
Optimization algorithm improvement	Na [11]	Gradient learning rate adaptive algorithm based on ADMM	This article uses ADMM for regional decentralized computing to reduce computational cost
Economic dispatch of power system	Shi et al [12]	Dynamic programming algorithm based on FRDDP	This article combines IBDR and ADMM to optimize scheduling cost
Load transmission of power distribution system	Jiang et al [13]	Three stage optimization algorithm	This article does not cover

ADMM, alternating direction multiplier; IBDR, incentive-based demand response.

the reliability of the power supply in the power system [13]. The summary of the above content and its comparison with the research content are shown in Table 1.

Based on the above content, it can be concluded that current research mainly focuses on the application technology of high-proportion renewable energy grid connection. However, the main research problem is the lack of global collaboration capability and only optimizing a single site, which makes it difficult to respond in real time to changes in distributed resources. Therefore, the research first establishes random fuzzy models for photovoltaic, wind power, gas, electricity, and heat loads, as well as energy hub control models in the system. Then, the various energy flows in the power system are modeled, and a new flow calculation method is established. Finally, a large-scale integrated power system scheduling model based on ADMM is designed. The innovation of the research lies in the ADMM algorithm for regional decentralized computing, which transforms the linear three-layer programming algorithm into a conventional two-layer programming algorithm, achieving the integrated scheduling requirements of source-grid-load-storage for the multi-regional, multi-power system under three-layer programming.

II. METHODS AND MATERIALS

The unstable output of new energy and the randomness of the electricity load end have led to difficulties in the integrated scheduling of multi-regional source-grid-load-storage in large-scale power systems. Therefore, the research establishes a control hub for source-grid-load-storage integrated scheduling and uses stochastic FT to compute the power flow of each part. The ADMM is used for decentralized computing of power system regions, which determines information exchange between regions, and improves computing efficiency, hoping to minimize the planning cost, operating cost, frequency control cost, and fluctuation of large-scale power systems.

A. *Design of Random Fuzzy Power Flow Algorithm Based on Semi-Invariant Method*

To achieve source-grid-load-storage integrated scheduling in large-scale power systems, an energy hub is established, which takes into account photovoltaic and wind power output, Electric Storage (ES), Power to Gas (P2G), WT, Combined Heat and Power (CHP), etc [14, 15]. The energy hub structure is displayed in Fig. 1.

In Fig. 1, the energy hub is linked to renewable energy equipment, including photovoltaics and wind power, as well as the user's load end. The power energy is transmitted through transformers in the middle, and the energy conversion between electrical and thermal rooms is completed through equipment such as CHP. For energy storage, equipment such as ES, HS (Heat Storage), GS (Gas Storage), etc., are used to store electrical and thermal energy. During energy hub operation, the gas supply allocation factor for photovoltaic and wind power is $\tilde{v}_{w,t}$. The distribution network and energy hub exchange power P_t with random fuzzy values in a given time interval t. The allocation factor during this period is $v_e(t)$. The electricity injected into the electrical conversion device by the distribution network and new energy is $v_e(t)\tilde{P}_e(t)$ and $v_w(t)\tilde{P}_w(t)$, respectively. Therefore, the coupling effect between the output and input of the energy hub in the t interval is shown in (1).

$$\begin{bmatrix} L_e(t) \\ L_h(t) \\ L_g(t) \end{bmatrix} = \begin{bmatrix} (1-v_w(t))\eta_{r-e} & \left(1-v_e(t)\right)\eta_{e-e} & \eta_{g-e} \\ 0 & 0 & \eta_{g-h} \\ v_w(t)\eta_{e-g} & v_e(t)\eta_{e-g} & 1 \end{bmatrix} \begin{bmatrix} \tilde{P}_w(t) \\ \tilde{P}_e(t) \\ \tilde{P}_g(t) \end{bmatrix} \quad (1)$$

In (1), $L_e(t)$, $L_h(t)$, $L_g(t)$ represent the output power of the electrical and thermal energy sources, respectively. The η_{e-g} shows the efficiency of converting electricity to gas. η_{g-h} and η_{g-e} are the efficiencies of gas-to-heat and gas-to-electricity conversion in energy conversion equipment, respectively. η_{r-e} is the efficiency of photovoltaics and WTs. When the energy hub considers energy storage in the source-grid-load-storage integrated scheduling, the extended expression of the coupling relationship is displayed in (2) [16].

$$\begin{bmatrix} L_e(t) \\ L_h(t) \\ L_g(t) \\ L_e'(t) \\ L_h'(t) \end{bmatrix} = \begin{bmatrix} \left(1-v_w(t)\right)\eta_{r-e} & \left(1-v_e(t)\right)\eta_{e-e} & \eta_{g-e} & 1 & 0 \\ 0 & 0 & \eta_{g-h} & 0 & 0 \\ v_w(t)\eta_{e-g} & v_e(t)\eta_{e-g} & 1 & 0 & 1 \\ \left(1-v_w(t)\right)\eta_{e-s} & \left(1-v_e(t)\right)\eta_{e-s} & 0 & 1 & 0 \\ 0 & 0 & \eta_{g-h}\eta_{h-s} & 0 & 1 \end{bmatrix} \begin{bmatrix} \tilde{P}_w(t) \\ \tilde{P}_e(t) \\ P_g(t) \\ \tilde{P}_e'(t) \\ P_h'(t) \end{bmatrix} \quad (2)$$

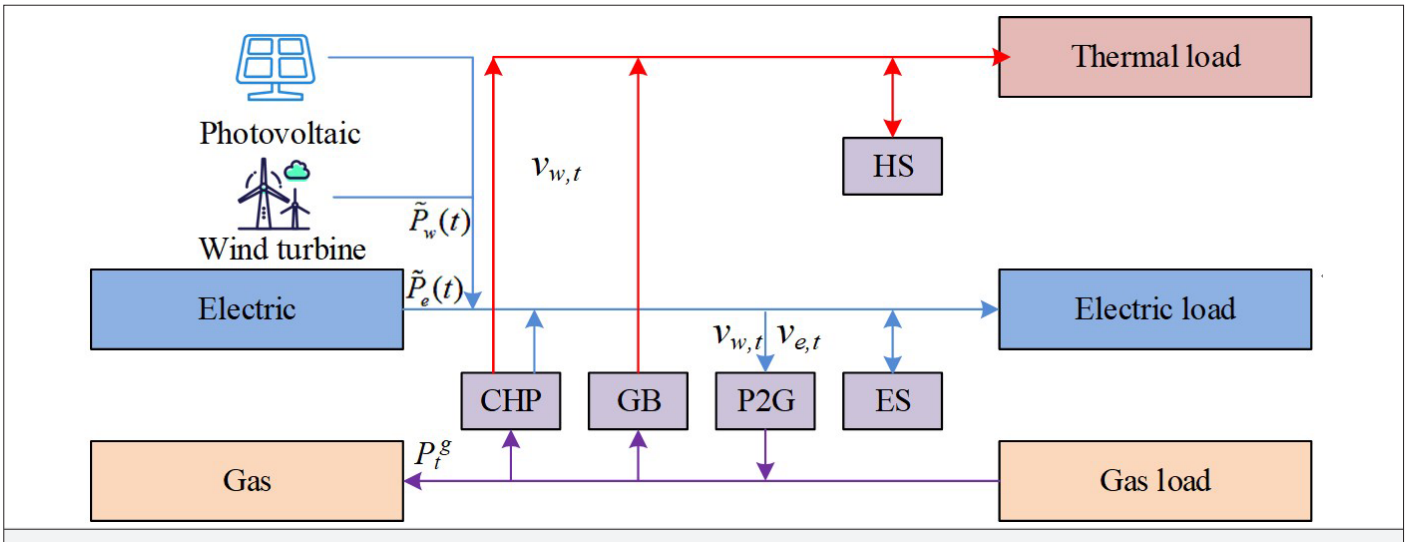

Fig. 1. Schematic diagram of energy hub structure.

In (2), η_{h-s} and η_{e-s} represent the energy storage efficiency of HS and ES, respectively. $P_h'(t)$ and $\tilde{P}_e'(t)$ represent the thermal and electrical energy reserves at the beginning of the time period t. $L_h'(t)$ and $L_e'(t)$ signify the thermal and electrical energy reserves at the end of time period t. Hybrid power flow calculation can understand the voltage magnitude and phase angle of each node, and the power flow of each line. Through power flow calculation, the system state is quantitatively assessed and the intelligent improvement of the power system can be achieved [17]. After completing the mathematical modeling of the energy hub, the mixed power flow calculation for large-scale power systems is performed to provide a foundation for subsequent implementation of source-grid-load-storage integrated scheduling. The power of power nodes in the power system is shown in (3).

$$\begin{cases} P = \mathrm{Re}\left\{\dot{U}\left(Y\dot{U}\right)^*\right\} \\ Q = \mathrm{Im}\left\{\dot{U}\left(Y\dot{U}\right)^*\right\} \end{cases} \tag{3}$$

In (3), $\dot{U}$ signifies the voltage vector. Y represents the admittance matrix. Q and p are the reactive power and active power of the node, respectively. The energy consumption for gas compressors in large-scale power systems is shown in (4).

$$\begin{cases} q_{fc} = \left(a_1 P_s^2 + a_2 P_s + a_3\right) / LHV \\ P_s = \dfrac{q_{in} Z_{in} T_{g,in} R_s \gamma}{\eta_{ad}\left(\gamma - 1\right)}\left[\left(\dfrac{p_{out}}{p_{in}}\right)^{(\gamma-1)/\gamma} - 1\right] \\ q_{out} = q_{in} - q_{fc} \end{cases} \tag{4}$$

In (4), q_{fc} represents the energy consumption power of the natural gas starting compressor. P_s is the energy consumption power of the motor-driven compressor. *LHV* represents the low calorific value of natural gas. p_{out} and p_{in} are the pressures at the inlet and outlet of the compressor, respectively. γ is the index of variability. $T_{g,in}$ represents the temperature of the gas. z_{in} represents the compression factor at the entrance. q_{in} represents the inlet flow rate. In the electric thermal collaborative network of large-scale power systems, the heat load and heat source in a steady state are shown in (5).

$$\Phi_{SP,i} = C_p L_{h,i}\left(T_{s,i} - T_{r,i}\right) \tag{5}$$

In (5), $T_{r,i}$ and $T_{s,i}$ are the return water temperature and hot water temperature of hot node i. $L_{h,i}$ signifies the node traffic. $\Phi_{SP,i}$ represents the thermal power of the node. The coupling of large-scale power systems is tight. The unified solution of power system flow ensures convergence, but it requires more computation and time. The decomposition solution method can decouple and solve independent subsystems until they all converge. Therefore, the research introduces the decomposition solution method for power flow calculation. The decomposition solution method is displayed in Fig. 2.

In Fig. 2, the decomposition solution method first decouples the energy hub, and then iteratively solves it in the electrical thermal network. Power flow mathematical models of each subsystem are established during the solving process. Finally, the mixed power flow of each subsystem is obtained by calculating the power flow mathematical model. The power flow calculation mathematical model in the decomposition solution method is shown in (6).

$$\begin{cases} P = \mathrm{Re}\left\{\dot{U}(Y\dot{U})^*\right\} = 0 \\ Q - \mathrm{Im}\left\{\dot{U}(Y\dot{U})^*\right\} = 0 \\ L - A_l q_g = 0 \\ B_g K_{r,g} q_g \left|q_g\right| = 0 \\ \Phi_{SP} - C_p A_l q\left(T_s - T_r\right) = 0 \\ B_h K_{r,h} q_h \left|q_h\right| = 0 \\ C_s T_{s,load} - b_s = 0 \\ C_r T_{r,load} - b_r = 0 \end{cases} \tag{6}$$

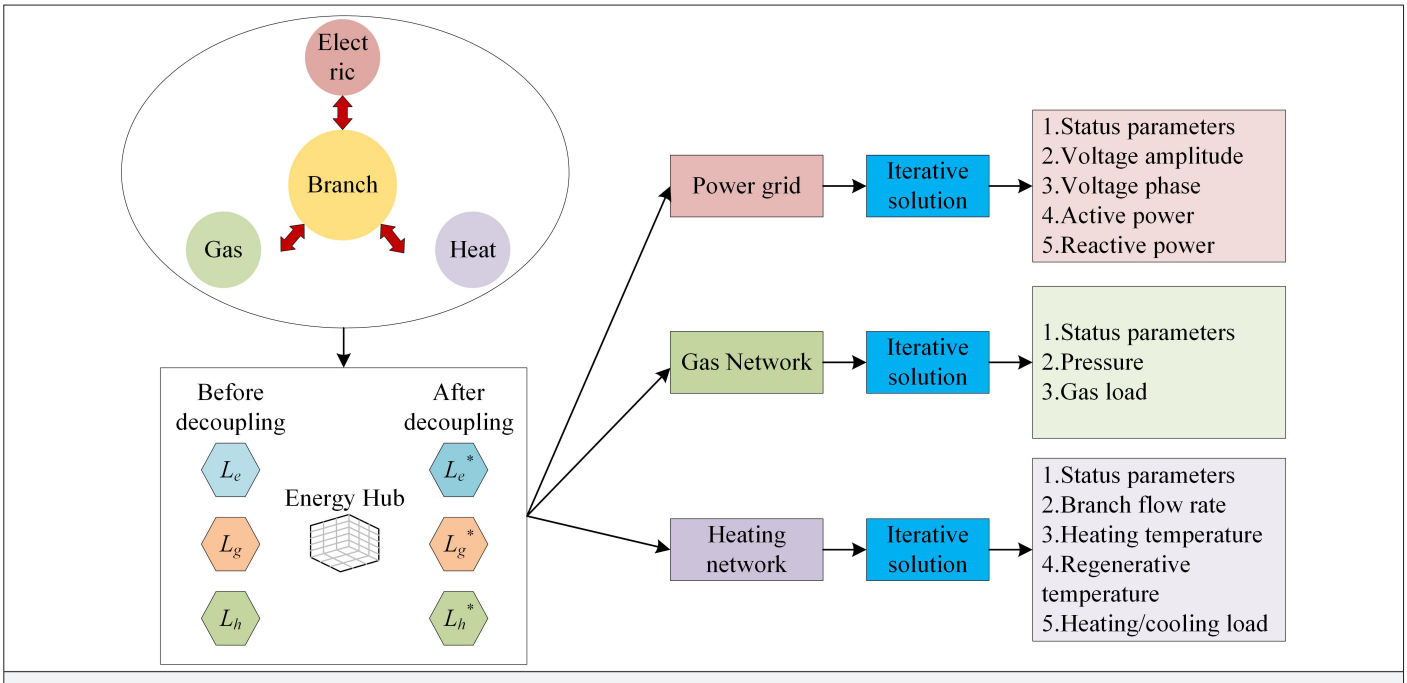

Fig. 2. Schematic diagram of decomposition solution method.

With the increasing integration of distributed new energy into the grid, the input of new energy with unstable output introduces ambiguity. The randomness of variables in power flow calculation can be considered through (6), but fuzziness is not taken into account. Therefore, fuzzy power flow is used to replace the probability power flow calculation method in (6), and the incremental method is adopted to deal with the ambiguity caused by distributed energy and other factors. The expression for calculating the fuzzy incremental value using the incremental method is shown in (7).

$$\begin{cases} \Delta\tilde{W} = \tilde{W}_i - W_{di} \\ \Delta\tilde{X} = J_0^{-1}\Delta\tilde{W} \\ \Delta Z = G_0 J^{-1}\Delta\tilde{W} \end{cases} \tag{7}$$

In (7), ΔZ is the fuzzy increment of pipeline flow and branch active and reactive power. $\Delta\tilde{X}$ signifies the increment of voltage amplitude, phase angle, air pressure, and return water temperature matching. ΔW signifies the increment of matching the fuzzy expected value of injection power. w_{di} is the result of deterministic power flow calculation. W_i is the fuzzy expected value of injected power for electrical, gas, and thermal nodes. The semi-invariant method is a commonly used algorithm for dealing with fuzziness and randomness in power systems. Based on semi-invariants to approximate probability distributions, it can reduce the computational cost of traditional convolution operations and enhance computational efficiency. Therefore, the calculation for solving the stochastic fuzzy power flow of large-scale power systems using the semi-invariant method is shown in (8).

$$\begin{cases} \tilde{X} = X_0 + S_0\Delta\tilde{W} \\ \tilde{Z} = Z_0 + T_0\Delta\tilde{W} \end{cases} \tag{8}$$

In (8), S_0 and T_0 signify sensitivity matrices, where 0 represents the reference operating point, and $S_0 = J_0^{-1}$ and $T_0 = G_0 J_0^{-1}$. For the sum of independent random variables, their respective order cumulants can be obtained by simply adding up the corresponding order cumulants of each independent random variable. The semi-invariant method transforms complex convolution problems into easier-to-handle arithmetic operations, thereby quickly obtaining the probability distribution of system state variables. The arithmetic operation is shown in (9).

$$\begin{cases} \Delta X^{(k)} = \tilde{S}^{(k)}\ \Delta\tilde{W}^{(k)} \\ \Delta\tilde{Z}^{(k)} = \tilde{T}^{(k)}\ \Delta\tilde{W}^{(k)} \end{cases} \tag{9}$$

In (9), $\Delta X^{(k)}$ and $\Delta Z^{(k)}$ signify the k-order semi-invariants of ΔX and ΔZ, respectively. $\tilde{w}^{(k)}$ signifies the k-order semi-invariant of the input variable w. The specific method of using the semi-invariant method to solve random fuzzy power flow is shown in Fig. 3.

In Fig. 3, firstly, all data in the large-scale power system is read to match the credible range of fuzzy parameters. Afterward, the mean of all possible distribution state variables is calculated, and the sensitivity at the benchmark running time is represented in matrix form. Finally, the fuzzy confidence interval and fuzzy power flow distribution are obtained by simplifying the operation of semi-invariants. The fuzzy power flow results and energy utilization of ENERGY HUB are outputs.

B. *Construction of Large-Scale Power System Source-Grid-Load-Storage Integrated Scheduling Model Based on Incentive-Based Demand Response–Alternating Direction Multiplier*

For the source-grid-load-storage integrated scheduling in the large-scale power system, power sources, grids, and storage can achieve power balance through the adjustment of the power system's own

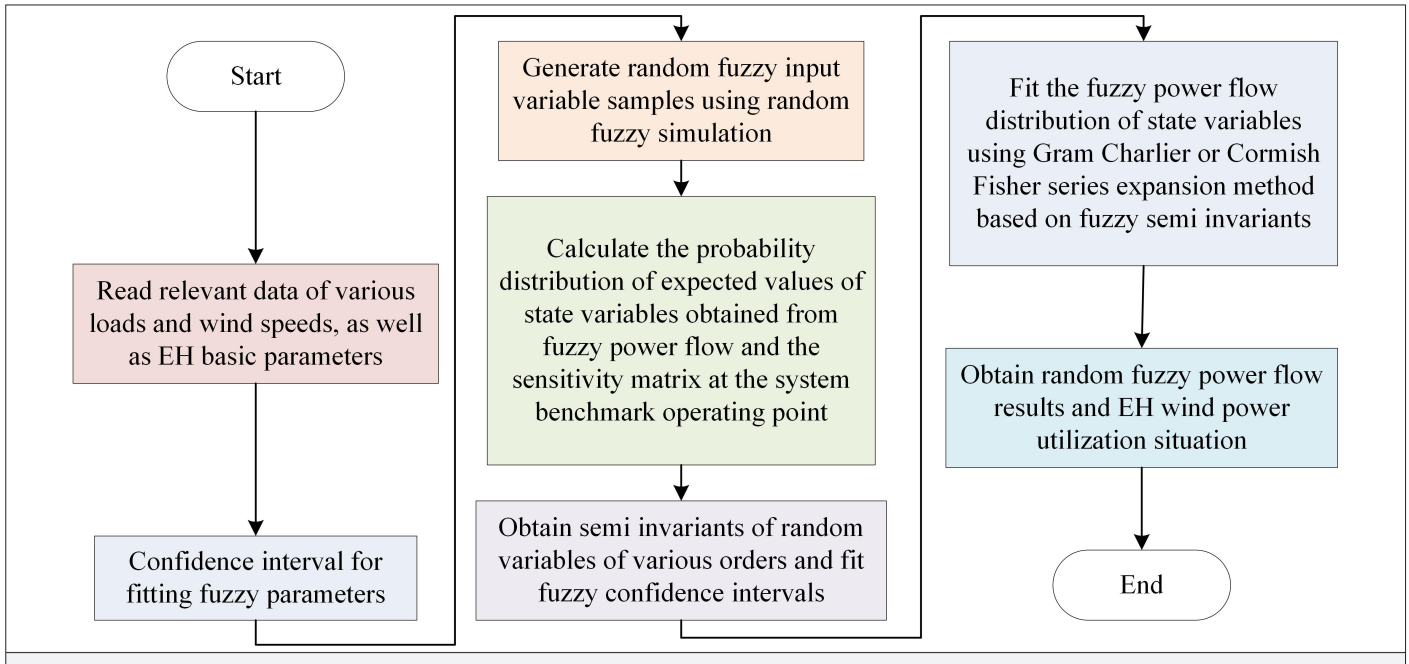

Fig. 3. Method of solving stochastic fuzzy power flow using the semi-invariant method.

equipment, but load-side scheduling can only respond and adjust from the user's demand side. Therefore, the research introduces Incentive-based Demand Response (IBDR) to reduce or transfer the load on the user side. The corresponding expression for IBDR is shown in (10).

$$\begin{cases} L_i'(t) = L_i(t) + P_i^{\mathrm{LRDR}}(t) + P_i^{\mathrm{LTDR}}(t) \\ P_i^{\mathrm{LRDR}}(t) \le 0 \\ \sum_{t=1}^{T} P_i^{\mathrm{LTDR}}(t) = 0 \end{cases} \tag{10}$$

In (10), T is the time period of the scheduling cycle. $L_i(t)$ and $L_i'(t)$ signify the load before and after participating in IBDR, respectively [18, 19]. $P_i^{\mathrm{LTDR}}(t)$ and $P_i^{\mathrm{LRDR}}(t)$ represent the load transfer amount and load reduction amount of node *i* during the *t* time period, respectively. To promote users' response to the demand for load transfer and reduction in the power system, appropriate compensation should be provided to users. The compensation cost C_{IBDR} is shown in (11).

$$C_{\mathrm{IBDR}} = \sum_i \sum_{t=1}^{T} \left(\mu_1 \left| P_i^{\mathrm{LRDR}}(t) \right| + \mu_2 \left| P_i^{\mathrm{LTDR}}(t) \right| \right) \tag{11}$$

In (11), μ_1 and μ_2 are the unit compensation costs for load transfer and reduction. In large-scale power system scheduling, due to the higher flexibility of thermal power units and energy storage equipment control, energy storage systems and thermal power units are used to undertake frequency regulation tasks. The Automatic Generation Control (AGC) of thermal power units is shown in (12).

$$\begin{cases} ACE_{FFC} = B \times \Delta f \\ ACE_{FTC} = \Delta P_T \\ ACE_{TBC} = B \times \Delta f + \Delta P_T \end{cases} \tag{12}$$

In (12), Δf represents the frequency deviation between regions. ΔP_T represents the power deviation value of the connecting line. *B* represents the frequency deviation coefficient [20, 21]. ACE represents the deviation that occurs in the control of the secondary frequency modulation area. ACE_{FFC}, ACE_{FTC}, and ACE_{TBC} represent three different control modes of AGC. The State of Charge (SOC) of the energy storage system during frequency regulation is shown in (13).

$$SOC = SOC_0 + \frac{\int_0^t P(k)dt}{E_M} \tag{13}$$

In (13), E_M signifies the total capacity of the energy storage system. $P(k)$ signifies the output power of the energy storage system at time k. SOC_0 is the initial value of the SOC [22]. The structural diagram of the energy storage system in grid frequency regulation is shown in Fig. 4.

In Fig. 4, the regional load variation in the power system is input to the energy storage system. The energy storage system calculates the frequency deviation coefficient B, generates the AGC control signal β for the power grid through B, and adopts β to compute the output power of the secondary frequency regulation to achieve power grid frequency regulation [23, 24]. The two-layer programming method is commonly used for power system scheduling, which achieves optimal programming through decision-making and parameter feedback of upper and lower layers. However, this method cannot meet the more complex scheduling requirements in large-scale power systems. Therefore, the research adopts a three-layer programming method to achieve complex scheduling requirements. The upper-layer programming is to minimize the cost within the cycle of a large-scale power system, and the objective function is displayed in (14).

$$\begin{aligned} min C_{\mathrm{inv},n}(y) = & \sum_{i \in IL} \mu_n^{IL} P_{i,n}^{IL,rate} I_{i,n}^{IL}(y) + \sum_{i \in type2} \mu_n^{ID} P_{i,n}^{ID,rate} I_{i,n}^{ID}(y) \\ & + \sum_{\mathrm{Gen}i} \mu_{\mathrm{Gen}i,n} P_{\mathrm{Gen}i,n}^{\mathrm{rate}} I_{\mathrm{Gen}i,n}(y), IL \in \Omega_{IL}, ID \in \Omega_{ID} \end{aligned} \tag{14}$$

In (14), *n* represents different regions of electricity. $\mu_{\mathrm{Gen}i,n}$ is the unit investment cost of the generator set. μ_n^{ID} and μ_n^{IL} are the unit planning costs for equipment, lines, and pipelines [25, 26]. $I_{\mathrm{Gen}i,n}$, $I_{i,n}^{ID}(y)$, and $I_{i,n}^{IL}(y)$ represent the planning situation of the line in the *y*-year. $P_{\mathrm{Gen}i,n}^{\mathrm{rate}}$ is the rated capacity of conventional generator units. $P_{i,n}^{ID,rate}$ and $P_{i,n}^{IL,rate}$ are the rated capacities of equipment, pipelines, and lines, respectively. The constraint is that duplicate construction is not allowed [27]. The middle-layer programming is to waken carbon emissions and the operating cost of the integrated energy system. The objective function calculation is shown in (15).

$$\begin{cases} \min F_{\mathrm{ope},n}(y) = \sum_{WTi} c_{WTi,n} P_{WTi,n}(y,t) + \sum_{PVi} c_{PVi,n} P_{PVi,n}(y,t) + \sum_{Geni} c_{Geni,n} P_{Geni,n}(y,t) + \\ \sum_{i \in ED} c_n^{ED} P_{i,n}^{ED}(y,t) + \sum_{GSi} c_{GSi,n} P_{GSi,n}(y,t) + C_{\mathrm{IBDR},n} + C_{\mathrm{carbon},n}, IL \in \Omega_{IL}, ID \in \Omega_{ID} \\ C_{\mathrm{carbon},n}(y) = \lambda_{CO_2} \left(\sum_{GENi} \xi_{GEni} P_{Geni,n}(y,t) + \sum_{GSi} \xi_{GSi} P_{GSi,n}(y,t) \right) \end{cases} \tag{15}$$

In (15), $P_{GSi,n}(y,t)$ represents the gas supply of a segment *t* in the *y*-th year. $P_{\mathrm{Gen}i,n}(y,t)$, $P_{PVi,n}(y,t)$, $P_{WTi,n}(y,t)$, and $P_{i,n}^{ED}(y,t)$ respectively

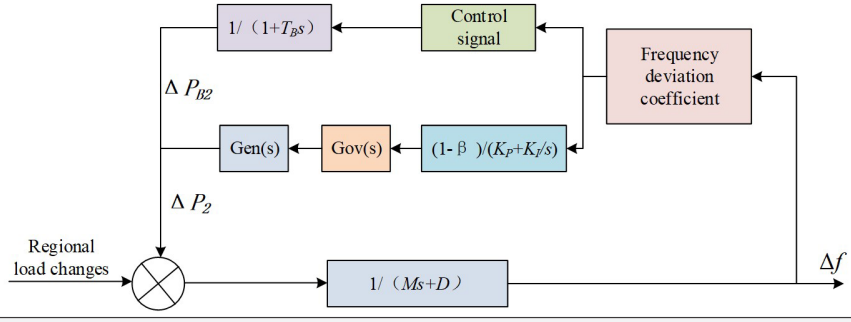

Fig. 4. Structural diagram of energy storage system in grid frequency regulation.

represent the output of conventional power generation units, photovoltaics, WTs, and energy storage and conversion equipment. $c_{GSi,n}$ is the unit cost of gas. c_n^{ED}, $c_{Geni,n}$, $c_{pvi,n}$, and $c_{WTi,n}$ respectively represent the unit cost of energy storage and conversion equipment, conventional power generation units, photovoltaic and WT operation. The constraints include capacity, demand balance, regional connectivity power constraints, etc. The lower-layer programming is to minimize frequency control cost and output variable fluctuations. The objective function is displayed in (16).

$$\min J_{con,n} = \left(\sum_{Geni} \gamma_G P_{Geni,n}(y,t) + \sum_{ESi} \gamma_S P_{ESi,n}(y,t)\right) + ACE \tag{16}$$

In (16), $P_{ESi,n}(y,t)$ is the energy storage frequency modulation output. The constraint conditions are system balance and safe power transmission of the line. The objective function of constructing a large-scale power system source-grid-load-storage integrated scheduling is transformed into a three-layer programming problem. The transmission relationship of the three-layer programming is shown in Fig. 5.

In Fig. 5, the upper, middle, and lower layers form a complete closed-loop scheduling model. The lower layer returns basic data such as frequency to the middle layer, and the middle layer returns the output results of the system equipment to the upper layer. The upper layer plans the scheduling scheme for a large-scale power system based on the output results, while the middle layer adjusts the output of each piece of equipment according to the scheme. The complex scheduling of large-scale power systems is achieved through three-layer programming, and distributed algorithms are often used for calculation during the solving process. ADMM is a simple distributed algorithm with fast convergence speed and high robustness.

The ADMM is used for decentralized solutions of various regions in the middle and lower layers. The objective function for the ADMM solution is shown in equation

$$\begin{cases} \min F = \sum_{n=1}^{A} F_{ope} \\ F_{ope,n} = \sum_{WTi} c_{WTi,n} P_{WTi,n}(y,t) + \sum_{Geni} c_{Geni,n} P_{Geni,n}(y,t) \\ \quad + \sum_{i \in ED} c_n^{ED} P_{i,n}^{ED}(y,t) + \sum_{GSi} c_{GSi,n} P_{GSi,n}(y,t) + C_{DR,n} \end{cases} \tag{17}$$

In (17), F represents the comprehensive operating cost. The process of using the ADMM algorithm for decentralized solution in each region is shown in Fig. 6.

In Fig. 6, the solving process of ADMM is as follows. The basic data, including load and equipment parameters, are first inputted. Then, initialization settings are made for each region, including determining the convergence boundary and the initial value of electrical conversion line power. Afterwards, the power variation value of the electrical interconnection line is obtained through distributed computing. In large-scale power systems, adjacent regions transmit updated values of variables and update the reference fixed values and multipliers within each region to achieve information exchange between regions. Finally, the algorithm will determine whether it converges, and if so, output a scheduling plan; otherwise, return to the distributed computing step to continue iterating. Through this distributed-solving approach, the ADMM algorithm can efficiently solve complex scheduling problems in large-scale power systems.

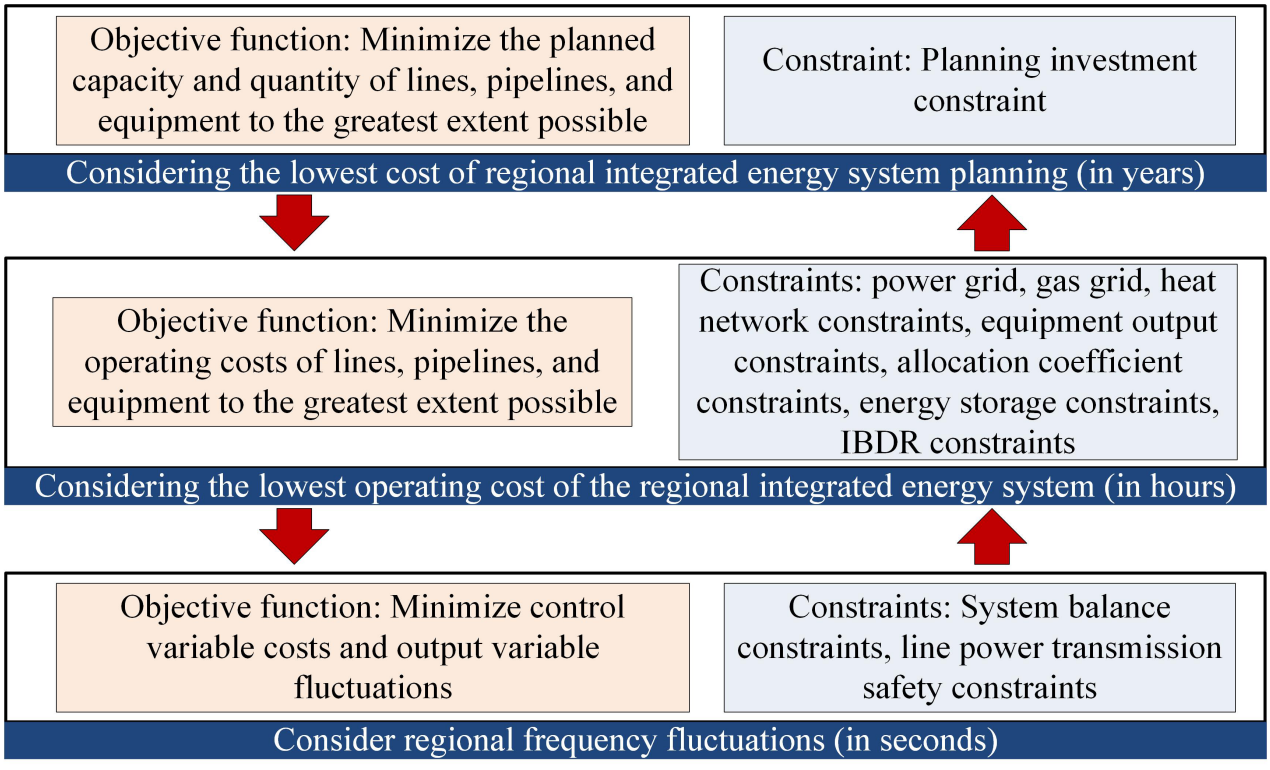

Fig. 5. Transmission relationship of three-layer programming.

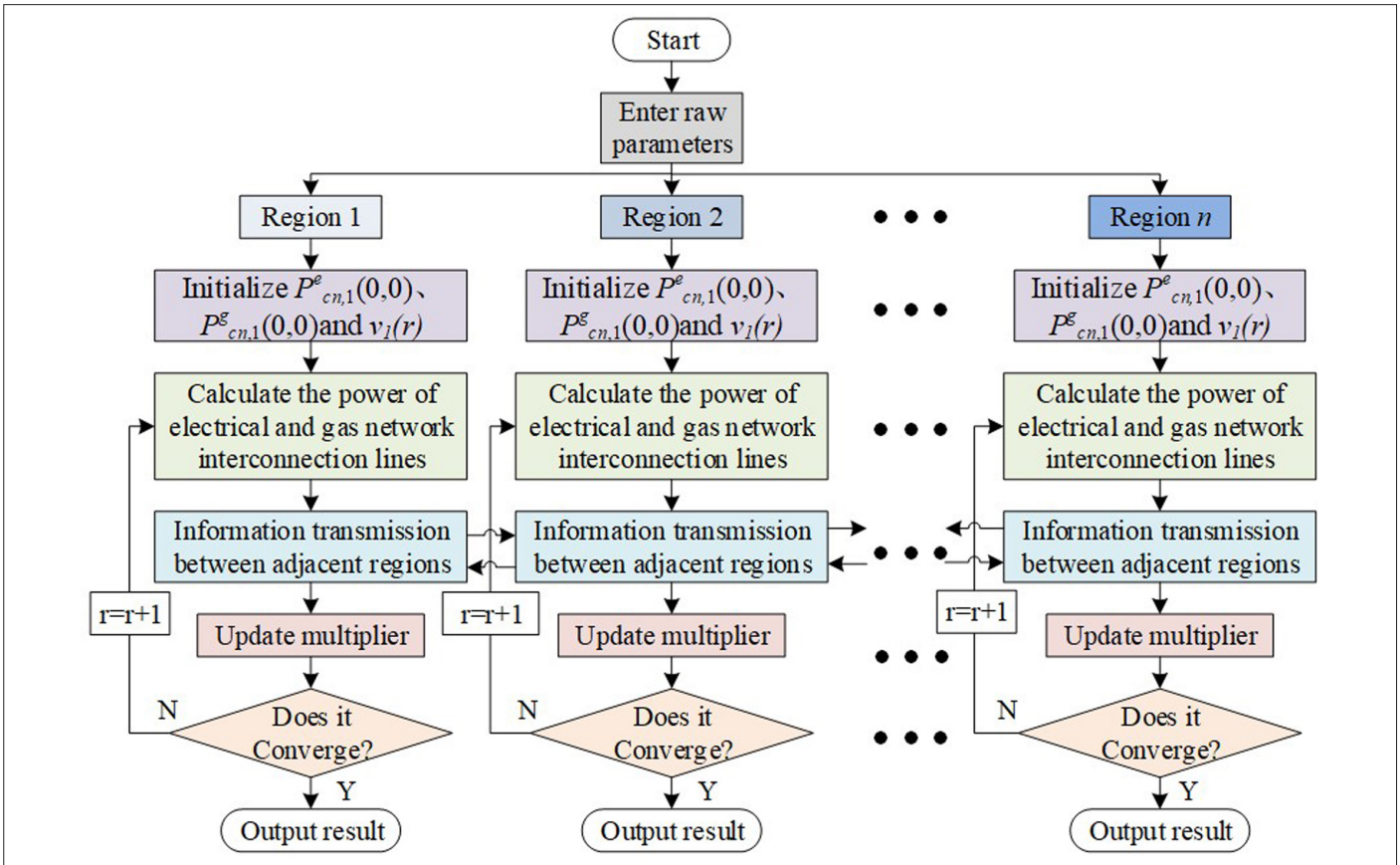

Fig. 6. Flowchart of alternating direction multiplier.

III. RESULTS

To demonstrate the performance of the model, relevant experiments are carried out. The experiment first conducts a comparative test on the random fuzzy power flow solving algorithm based on the semi-invariant method, testing the reliability of the algorithm for power system scheduling decisions. Then, a simulation experiment is established to simulate the integrated scheduling of source-grid-load-storage in large-scale power systems. Comparative experiments are conducted in different regions and environments for the source-grid-load-storage to analyze the model's effectiveness. Finally, a comparative experiment is conducted between the research model and the comparative method in the large-scale power system based on the generalized Benders decomposition algorithm to verify the performance of the research model.

A. *Testing of Random Fuzzy Power Flow Solving Algorithm Based on Semi-Invariant Method*

A comparative test is conducted between the random fuzzy power flow solving algorithm based on semi-invariant method and the random power flow solving algorithm to compute the mixed power flow of the simulated system. The simulated mobile system being tested is a multi-energy system composed of an IEEE 39 node New England power system, a 14 node thermal system, and a 14 node Belgian natural gas system coupled together, with each coupled node serving as an energy hub. Meanwhile, the wind speed data of the wind farm and the data of the photovoltaic power station are collected on a 30-day cycle, with 24 time periods per day and 3 data points collected in each time period. The simulation software uses MATLAB R2023a, with an Intel Xeon Gold 6248 processor, 2.5GHz, 128 GB memory, and a Windows 10 operating system. The

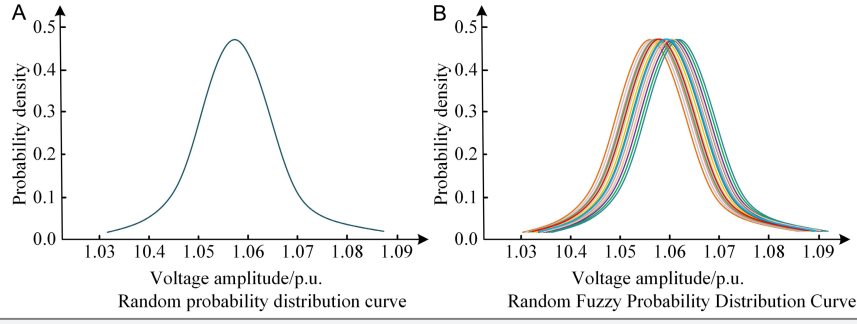

Fig. 7. Probability distribution curve of voltage amplitude for a single node.

probability distribution of the voltage amplitude for a single node in the system is shown in Fig. 7.

According to Fig. 7 (a) and Fig. 7 (b), the maximum probability density in the voltage amplitude curves calculated by both algorithms was close to 0.47, and the curve trend remained consistent. There was only one probability distribution curve in Fig. 7 (a), while the curve in Fig. 7 (b) was a group of equally possible lines. The results indicate that scheduling solely based on randomness may deviate from reality while calculating fuzzy probability power flow can obtain a probability density curve decision set, which is a more reasonable basis for scheduling decisions. In large-scale power systems, the output of new energy sources such as photovoltaics and wind power is highly uncertain and ambiguous. The random fuzzy power flow algorithm can more accurately describe these uncertainties by introducing FT, thereby improving the reliability of scheduling decisions.

B. *Simulation Analysis of Source-Grid-Load-Storage Integrated Scheduling for Large-Scale Power System*

To verify the model, simulation experiments are carried out using three regions to simulate large-scale power systems. Region III includes the thermal, natural gas, and power systems of IEEE 7, 5, and 6 nodes. Regions I and II contain IEEE 15 node natural gas systems, 40 node power systems, and 13 node thermal systems. The annual growth rates of gas, heat, and electricity loads are 2%, 3%, and 5%. Four simulation experimental scenes are set up for comparative experiments. Scene 1 separates regions I, II, and III for three-layer scheduling programming but does not consider the load side IBDR. In scene 2, three regions are coordinated for scheduling, considering two-layer programming and not considering IBDR. In scene 3, three regions are coordinated for scheduling, considering three-layer scheduling but not IBDR. In scene 4, three regions are planned collaboratively, considering three-layer scheduling and load side IBDR, which is the scheduling model designed for research. The joint scheduling programming of multiple regions is shown in Table 2.

In Table 2, due to independent programming, scene 1 added generators and transmission lines to meet the load. In scene 2, frequency control is not considered under the two-layer programming, reducing the number of generators and energy storage devices. Scene 3 added ES to assist in frequency regulation and suppress fluctuations in new energy output. In scene 4, IBDR reduced the load and correspondingly reduced the power lines. The cost composition and new energy consumption of large-scale power systems after completing scheduling programming in four different environments are shown in Fig. 8.

TABLE II. MULTI-REGION JOINT DISPATCH PROGRAMMING

Scene	Energy Hub	Transmission Line	Alternator
Scene 1	CHP1(4), GB3(6)	1–4(2)	G4(2)
Scene 2	3-6(4) CHP1(4), GB3(6), HS1(3)	2–3(4), 1–4(2), 3–6(4)	/
Scene 3	CHP1(4), GB3(6), ES1(4), ES2(4), HS1(3)	1–4(2)	G4(2)
Scene 4	CHP1(6), ES1(4), ES2(4)	1–4(4)	G4(4)

In Fig. 8 (a), the cost composition of large-scale power systems under different scheduling environments was demonstrated. Each bar chart represents a scheduling environment, and the height of the bar chart represents the total cost. The different colors or symbols in the figure distinguish the cost components in different environments, including investment cost, operating cost, compensation cost, and frequency modulation cost. Among them, the single cost under scene 1 was the highest, with a total cost of 20 286.83 × 10^6 RMB. The total cost under scene 2 was 18 861.9 × 10^6 RMB. Considering collaboration and frequency control in scene 3, the total cost was lower than in scene 1 but higher than in scene 2. By implementing demand-side management in scene 4, the total cost was reduced to a minimum of 18 023.5 × 10^6 RMB. In Fig. 8 (b), the abandoned wind and solar rates were highest in scene 1, while they were lowest in scene 4, at 7.4% and 2.6%, respectively. From an economic perspective, the research method introduces IBDR and three-layer programming to more effectively coordinate scheduling strategies across regions, optimize resource allocation, and achieve significant cost reductions. This indicates that it can reduce unnecessary equipment investment and operating costs and significantly improve the economic efficiency of the system. The load adjustment of IBDR in each region in scene 4 is shown in Fig. 9.

In Fig. 9, the three bars in each group represent regions I, II, and III, and Fig. 9 shows the IBDR load adjustment in the three regions in scene 4. Fig. 9 (a) shows the load transfer situation, and Fig. 9 (b) shows the load reduction situation. In Fig. 9 (a), the fluctuation of load transfer was relatively large, with a maximum value of 12.2 MW and a minimum value of −13.3 MW. In Fig. 9 (b), the fluctuation of load reduction was relatively small. From Fig. 9 (a) and Fig. 9 (b), the load transfer and reduction in region III were not as good as those in regions I and II. The results indicate that through the participation of IBDR, the research model can effectively adjust the load, promote the consumption of new energy electricity, and reduce frequency

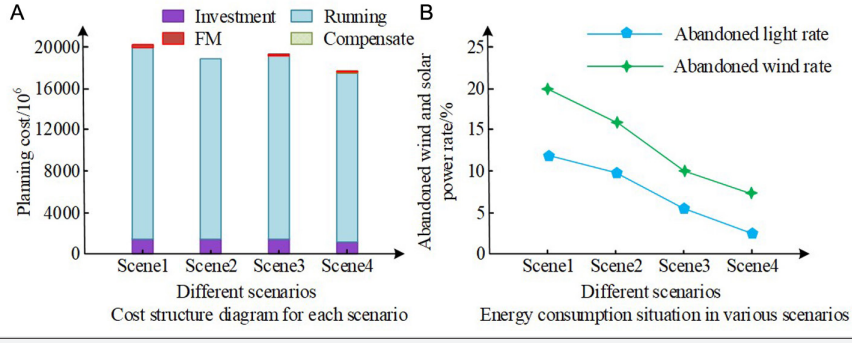

Fig. 8. System cost composition and new energy consumption.

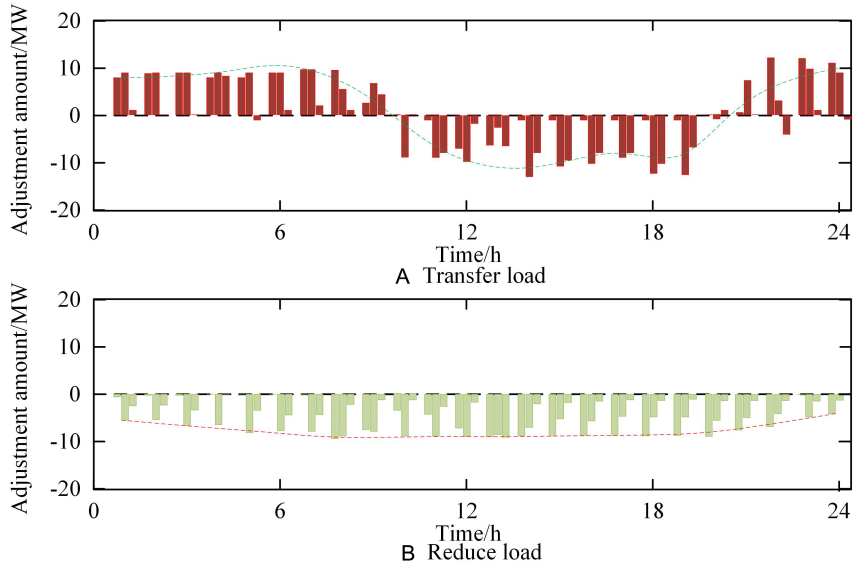

Fig. 9. Incentive-based demand response load adjustment in each area in scene 4.

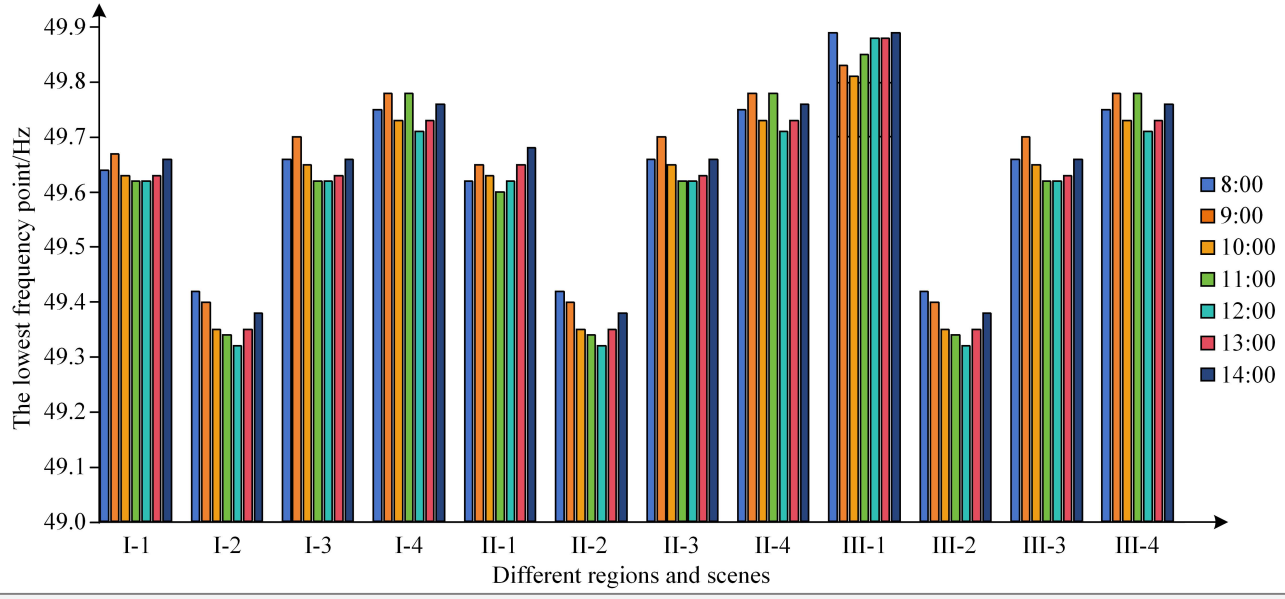

Fig. 10. Frequency lowest point deviation.

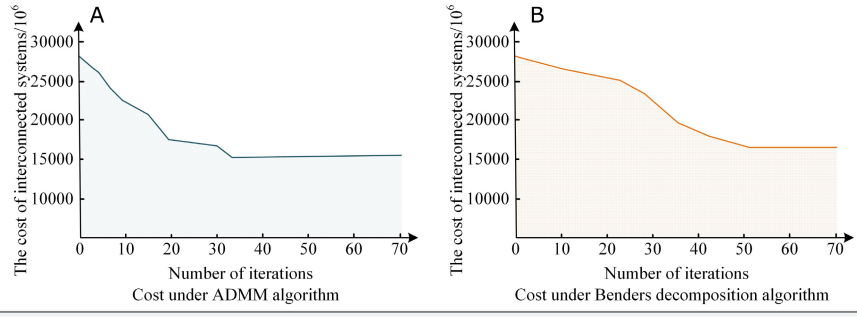

Fig. 11. Comparison test results of the power system scheduling model.

decline, thereby improving the stability and economy of the power system. From a social perspective, this research method can alleviate the load pressure on the power grid during peak hours, effectively improve user satisfaction, and ensure the safe operation of the power system. Fig. 10 shows the deviation of the lowest frequency points from 8 to 14 in the three regions during the peak shaving period under four different scenes.

In Fig. 10, in scene 1, the frequencies of regions I and II stabilized at 49.60–49.70 Hz, with region III having a slightly higher frequency. In scene 2, regional collaborative programming was carried out, but the lowest frequency of 49.3 Hz exceeded the normal range. Scene 3 considered frequency control to increase the frequency at the lowest point to the normal range. In scene 4, the frequency remained stable at around 49.72 Hz. From this, under the scheduling of the research model, the participation of IBDR further stabilizes frequency regulation in multiple regions, and demand response helps to reduce frequency drops. To further validate the research model, a comparative test is designed between the large-scale power system scheduling model based on the Benders decomposition algorithm and the research model, as displayed in Fig. 11.

In Fig. 11 (a), the research model achieved convergence after 33 iterations, with an optimal cost of 15 015 $\times$ 10^6 RMB. In Fig. 11 (b), the Benders model converged after 51 iterations, and the optimal cost was 11.7% higher than the research cost. From this, the research model is more in line with the requirements of source-grid-load-storage integrated scheduling in the large-scale power system than the Benders model. The summary of the above results is shown in Table 3.

TABLE III. THE SUMMARY OF THE ABOVE RESULTS

Figs.	Comparison Items	Indicator Situation
Fig. 7	Random flow solving algorithm	A group of equally possible curves
	Random fuzzy power flow solving algorithm	A group of equally possible lines is a more reasonable curve decision set
Fig. 8(a)	Scene I	20 286.83 × 10^6
	Scene 2	18 861.9 × 10^6
	Scene 3	19 354.1 × 10^6
	Scene 4	18 023.5 × 10^6
Fig. 8(b)	Scene I Abandoned light rate	12.1%
	Scene 2 Abandoned light rate	9.9%
	Scene 3 Abandoned light rate	5.1%
	Scene 4 Abandoned light rate	2.6%
	Scene I Abandoned wind rate	20.0%
	Scene 2 Abandoned wind rate	16.3%
	Scene 3 Abandoned wind rate	10.2%
	Scene 4 Abandoned wind rate	7.4%
Fig. 9(a)	Maximum load transfer value	12.2MW
	Minimum load transfer value	−13.3MW
Fig. 9(b)	Maximum load reduction	−4.6MW
	Minimum load reduction value	−8.2MW
Fig. 10	Scene I Region I	49.60~49.70Hz
	Scene I Region II	49.60~49.70Hz
	Scene I Region III	49.80~49.90Hz
	Scene 2 Region I	49.30~49.42Hz
	Scene 2 Region II	49.30~49.40Hz
	Scene 2 Region III	49.30~49.41Hz
	Scene 3 Region I	49.60~49.70Hz
	Scene 3 Region II	49.60~49.70Hz
	Scene 3 Region III	49.60~49.70Hz
	Scene 4 Region I	49.70~49.80Hz
	Scene 4 Region II	49.70~49.80Hz
	Scene 4 Region III	49.70~49.80Hz
Fig. 11	ADMM optimal cost	15 015 × 10^6
	Benders optimal cost	16 772 × 10^6

IV. DISCUSSION

The research conducted relevant tests and simulation experiments on the ADMM-based large-scale integrated scheduling model. The test results showed that the maximum probability density of the random fuzzy power flow solving algorithm based on semi-invariant was close to 0.47, and the probability distribution curve was a group of equally possible lines. This result was similar to the unified iterative power flow calculation method proposed by Yang et al., which considered the control mode of voltage source converters [28]. The research method had the lowest abandoned wind and solar rates, which were 7.4% and 2.6%, respectively. The fluctuation of load transfer was large, and the fluctuation of load reduction was small. The frequency during peak shaving periods remained stable at around 49.72 Hz. From this, under the scheduling of the research model, the load transfer in regions I and II promoted the consumption of new energy electricity, and the IBDR helped to reduce frequency drops. Ramachandran et al. obtained similar results in improving energy utilization efficiency through source-grid-load-storage integrated scheduling [29]. The research model converged after 33 iterations, with an optimal cost of 15 015 $\times$ 10^6 RMB, which was 11.7% lower than the Benders model. This result was similar to the research on IBDR improving power system efficiency and reliability drawn by Duc et al [30]. The results indicate that the random fuzzy power flow solving algorithm can improve the reliability of scheduling decisions, while the decentralized solving method in each region has higher computational efficiency and scheduling cost control performance.

V. CONCLUSION

The research is to address the scheduling challenges brought by the increasing demand for electricity and the widespread access of distributed new energy to the power system. A large-scale power system source-grid-load-storage integrated scheduling model based on ADMM was designed. An energy control hub was established, and random fuzzy power flow calculations were conducted. The ADMM

algorithm was used for regional decentralized computation in three-layer scheduling programming. An intelligent scheduling model based on ADMM was designed. Simulation experiments demonstrate that the model can effectively reduce cost, improve the absorption rate and frequency stability of new energy, and achieve intelligent source-grid-load-storage integrated scheduling in large-scale power systems. However, the research still has certain limitations, as it ignores the role of the correlation between loads in the programming results. In future research, the correlation among electricity load, heat load, and natural gas load can be comprehensively considered to improve the impact of correlation on the programming model.

Data Availability Statement: The data that support the findings of this study are available on request from the corresponding author.

Peer-review: Externally peer-reviewed.

Author Contributions: Concept – Q.D.L., Y.W.; Design – C.L.Z., D.Y.Z.; Supervision – Q.D.L.; Resources – Q.D.L.; Materials – Y.W., D.Y.Z.; Data Collection and/or Processing – Q.D.L., Y.W., C.L.Z.; Analysis and/or Interpretation – Y.W., C.L.Z., D.Y.Z.; Literature Search – D.Y.Z.; Writing – Q.D.L.; Critical Review – Q.D.L., Y.W., C.L.Z., D.Y.Z.

Declaration of Interests: The authors have no conflicts of interest to declare.

Funding: The authors declare that this study received no financial support.

REFERENCES

1. H. Yu, C. Ye, Y. Ding, and Y. Song, "Power system optimal dispatch integrating the responsive high-speed train fleet," *IEEE Trans. Smart Grid*, vol. 16, no. 1, pp. 728–740, 2025. [CrossRef]
2. B. Li, J. Zhao, Y. Zhang, and X. Bai, "Optimal configuration and economic operation of wind-solar-storage complementary system for agricultural irrigation in mountainous areas," *J. Electr. Eng. Technol.*, vol. 18, no. 4, pp. 2649–2666, 2023. [CrossRef]
3. K. Gairaa, C. Voyant, G. Notton, S. Benkaciali, and M. Guermoui, "Contribution of ordinal variables to short-term global solar irradiation forecasting for sites with low variabilities," *Renew. Energy*, vol. 183, no. 1, pp. 890–902, 2022. [CrossRef]
4. H. Xia, M. Pi, L. Jin, R. Song, and Z. Li, "Human collaborative control of lower-limb prosthesis based on game theory and fuzzy approximation," *IEEE Trans. Cybern.*, vol. 55, no. 1, pp. 247–258, 2025. [CrossRef]
5. F. Veshki, and S. Vorobyov, "Efficient ADMM-based algorithms for convolutional sparse coding," *IEEE Signal Process. Lett.*, vol. 29, no. 1, pp. 389–393, 2022. [CrossRef]
6. Y. Gao, Q. Ai, M. Yousif, and X. Wang, "Source-load-storage consistency collaborative optimization control of flexible DC distribution network considering multi-energy complementarity," *Int. J. Electr. Power Energy Syst.*, vol. 107, no. 5, pp. 273–281, 2019. [CrossRef]
7. C. Wang, X. Li, T. Tian, X. Zhi, and C. Ran, "Coordinated control of passive transition from grid-connected to islanded operation for three/single-phase hybrid multi-microgrids considering speed and smoothness," *IEEE Trans. Ind. Electron.*, vol. 67, no. 3, pp. 1921–1931, 2019.
8. Z. Echreshavi, M. Farbood, M. Shasadeghi, and S. Mobayen, "Reliable fuzzy control of uncertain nonlinear networked systems under actuator faults," *ISA Trans.*, vol. 141, pp. 157–166, 2023. [CrossRef]
9. L. Shano, T. K. Raghuvanshi, and M. Meten, "Fuzzy set theory and pixel-based landslide risk assessment: The case of Shafe and Baso catchments, Gamo highland, Ethiopia," *Earth Sci. Inform.*, 2022(2), vol. 15, no. 2, pp. 993–1006, 2022. [CrossRef]
10. G. Bai, Y. Feng, S. Huang, and P. Wang, "Distributed coordinated control method with multiple objectives optimization algorithm for wind farms," *IET Renew. Power Gener.*, vol. 17, no. 5, pp. 1068–1077, 2023. [CrossRef]
11. G. S. Na, "Efficient learning rate adaptation based on hierarchical optimization approach," *Neural Netw.*, vol. 150, no. 1, pp. 326–335, 2022. [CrossRef]
12. Y. Shi, C. Guo, S. Dong, C. Guo, Z. Chen, and L. Wang, "Enhancing the flexibility of storage integrated power system by multi-stage robust dispatch," *IEEE Trans. Power Syst.*, vol. 36, no. 3, pp. 2314–2322, 2020.
13. W. Jiang, L. Wu, L. Zhang, and Z. Jiang, "Research on load transfer strategy optimisation with considering the operation of distributed generations and secondary dispatch," *IET Generation Trans. & Dist.*, vol. 14, no. 23, pp. 5526–5535, 2020. [CrossRef]
14. Z. Li, T. He, and H. Farjam, "RETRACTED: Application of an intelligent method for hydrogen-based energy hub in multiple energy markets," *Int. J. Hydrog. Energy*, vol. 48, no. 93, pp. 36485–36499, 2023. [CrossRef]
15. S. Xi, H. Wu, Y. Mao, T. Wu, G. Song, JS. Terzic, and M. Shahidehpour, "Photovoltaic power generation and energy storage capacity cooperative planning method for rail transit self-consistent energy systems considering the impact of DoD," *IEEE Trans. Smart Grid*, vol. 16, no. 1, pp. 665–677, 2025. [CrossRef]
16. J. M. Pedraza, "The role of renewable energy in the transition to green, low-carbon power generation in Asia," *Green Low-Carbon Econ.*, vol. 1, no. 2, pp. 68–84, 2023. [CrossRef]
17. J. S. De, F. Gielnik, F. Mueller, and L. Schmit, "Suriyah M, Leibfried T. Physics-informed geometric deep learning for inference tasks in power systems," *Electr. Power Syst. Res.*, vol. 211, no. 1, pp. 1–8, 2022.
18. V. C. Pandey, N. Gupta, K. R. Niazi, A. Swarnkar, and R. A. Thokar, "Modeling and assessment of incentive based demand response using price elasticity model in distribution systems," *Electr. Power Syst. Res.*, vol. 206, no. 5, pp. 1–17, 2022. [CrossRef]
19. G. H. E. Gendolla, "Affective influences on the intensity of mental effort: 25 years of programmatic research," *Emot. Rev.*, vol. 17, no. 1, pp. 46–63, 2025. [CrossRef]
20. I. Kasireddy, A. W. Nasir, and A. K. Singh, "Application of FOPID-FOF controller based on IMC theory for automatic generation control of power system," *IETE J. Res.*, vol. 68, no. 3, pp. 2204–2219, 2022. [CrossRef]
21. R. Verma, S. K. Gawre, N. P. N. S. Patidar, and S. Nandanwar, "A state of art review on the opportunities in automatic generation control of hybrid power system," *Electr. Power Syst. Res.*, vol. 226, no. 1, pp. 1–17, 2024. [CrossRef]
22. K. Thangaraj, R. Indiran, V. Ananth, and M. Raman, "Enhanced lithium-ion battery state-of-charge estimation for Electric Vehicles using the AOA-DNN approach," *Optimal Control Appl. Methods*, vol. 45, no. 6, pp. 2856–2873, 2024. [CrossRef]
23. M. Yasin, and M. J. Khan, "Development of blind algorithm with automatic gain control," *Wirel. Netw.*, vol. 26, no. 4, pp. 2413–2422, 2020. [CrossRef]
24. R. R. Kibbe, and D. C. Muddiman, "Achieving sub-parts-per-million mass measurement accuracy on an Orbitrap mass spectrometry imaging platform without automatic gain control," *J. Am. Soc. Mass Spectrom.*, vol. 34, no. 6, pp. 1015–1023, 2023. [CrossRef]
25. S. Majumder, "Premium power investment strategy utilizing the economy of scale of custom power devices," *Electr. Power Syst. Res.*, vol. 214, no. 1, pp. 1–8, 2023. [CrossRef]
26. F. Ji, L. Gao, and C. Lin, "Lagrangian Modelling and motion stability of synchronous generator-based power systems," *CSEE J. Power Energy Syst.*, vol. 11, no. 1, pp. 13–23, 2025.
27. R. Aazami, H. Iranmehr, J. Tavoosi, A. Mohammadzadeh, M. H. Sabzalian, and M. S. Javadi, "Modeling of transmission capacity in reserve market considering the penetration of renewable resources," *Int. J. Electr. Power Energy Syst.*, vol. 145, no. 1, pp. 1–12, 2023. [CrossRef]
28. G. Yang, P. Dong, M. Liu, and H. Wu, "Research on random fuzzy power flow calculation of AC/DC hybrid distribution network based on unified iterative method," *IET Renew. Power Gener.*, vol. 15, no. 4, pp. 731–745, 2021. [CrossRef]
29. S. Ramachandran, and M. Ramasamy, "Solar photovoltaic interfaced quasi impedance source network based static compensator for voltage and frequency control in the wind energy system," *J. Electr. Eng. Technol.*, vol. 16, no. 3, pp. 1253–1272, 2021. [CrossRef]
30. T. Nguyen Duc, S. Tran Thanh, L. Do Van, N. Tran Quoc, and H. Takano, "Impact of renewable energy integration on a novel method for pricing incentive payments of incentive-based demand response program," *IET Generation Trans. & Dist.*, vol. 16, no. 8, pp. 1648–1667, 2022. [CrossRef]

Luo Qideng (1992.11 -), is currently engaged in grid planning research, grid project management, energy and power policy research, and research on source-grid-load-storage integration.

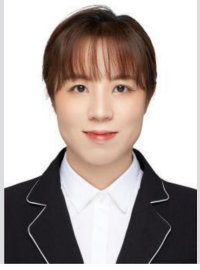

Wu Yue (1987.5 -), currently engaged in power grid planning, responsible for load forecasting, transmission network planning studies under the jurisdiction of the work.

Zhou Chunli (1988.1 -), is currently engaged in grid planning research, electric-carbon electric-hydrogen coupling research, and energy and power policy research.

Zhu Deyan (1981.5 -) is currently engaged in power system reform related issues and power grid planning and construction related issues, etc., and has been awarded the title of South Grid Women's Pioneer.